Struct Multidisc Optim (2015) 51:515–531
DOI 10.1007/s00158-014-1139-2

INDUSTRIAL APPLICATION

Structural design of a level-luffing crane through trajectory optimization and strength-based size optimization

Dong Soo Kim · Jongsoo Lee

Received: 12 December 2013 / Revised: 23 June 2014 / Accepted: 9 July 2014 / Published online: 31 July 2014

Abstract The present study explores the trajectory optimization of a double-rocker four-bar mechanism to minimize the amplitude of its trajectory. A numerical model of the levelluffing crane (LLC) is first developed to describe the trajectory mechanism, and the optimal trajectory is then identified after selecting dominant design variables in the context of design of experiments. The numerical optimization solution obtained is compared with measured data. The optimized trajectory design is then applied to the strength-based deterministic optimization (DO) to minimize the weight of a double-rocker structure under the constraints of stress and deflection. To carry out approximate optimization, a response surface method based on a second-order polynomial is used. Due to the existence of design uncertainties in an actual environment, reliability based design optimization (RBDO) is explored to assess the probabilities of failure in stress and deflection. For the design safety, DO and RBDO solutions are evaluated under severe loading conditions.

Keywords Double-rocker · Level-luffing crane · Trajectory mechanism · Design of experiments · Response surface method · Deterministic optimization · Reliability based design optimization

1 Introduction

This paper discusses a method to optimize the trajectory of a double-rocker four-bar mechanism in its application of the level-luffing crane (LLC). First, a numerical model (Cabrera et al. 2002; Acharyya and Mandal 2009) is developed to determine the trajectory. For the structural aspects in the curved trajectory of a double-rocker, its vertical amplitude should be as small as possible with satisfying the tolerance range over the horizontal moving distance between vessel and port. Second, the optimal curved trajectory should be identified by considering both the moving distance and amplitude of trajectory. The aim is to determine the actual model on the basis of the length of each link obtained through kinematic optimization. Afterwards, the model is applied to the level-luffing crane, a type of harbor equipment used for loading and unloading portage between the vessel and the ground, as shown in Fig. 1 (a) shows how the equipment has been operated for more than 20 years since its installation at the Mokpo Coal Quay, Jeonnam, Korea 2013. The LLC specifications include a rated capacity of 10 ton, a total weight of 350 ton, a height of 35 m, a maximum operating radius of 38 m, and a minimum operating radius of 14 m. Fig. 1(b) is a computer-aided drawing of the equipment, including the name of each part. The study of this equipment may be divided into a study of the composition of the links and a structural evaluation.

The composition of this double-link equipment has been described in previous studies (Moon et al. 2009; Hur et al. 2011), with changes in the link composition analyzed in terms of changes in the parameters that describe the design of the LLC equipment. Next, fatigue analysis and evaluation of the design's reliability (Xie et al. 2010) as well as its structural soundness (Kim et al. 2008) have been assessed in structure-related studies. In the fatigue analysis, first the design cycle spectrum is calculated, and then the stress spectrum of the structural block is evaluated using the load combination of fatigue in each cycle territory. The remaining life of the structure has been predicted by calculating

D. S. Kim · J. Lee (✉)
School of Mechanical Engineering, Yonsei University,
Seoul, 120–749, Korea
e-mail: jleej@yonsei.ac.kr

Fig. 1 Structure of level luffing crane

(a) General view of level luffing crane [3]

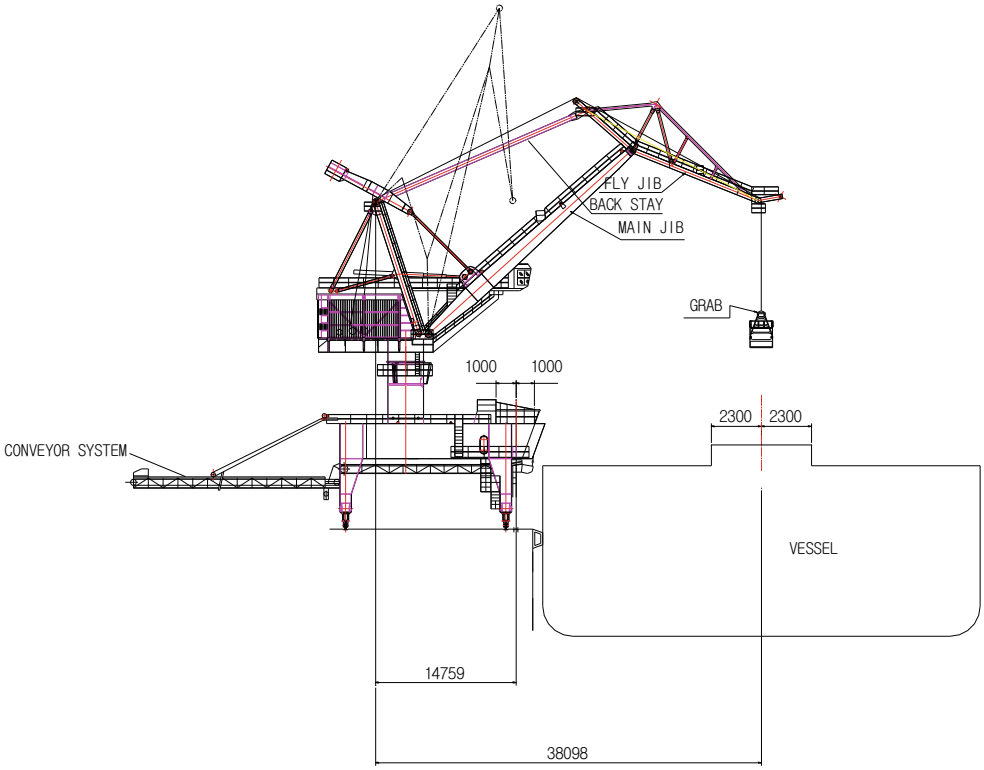

(b) Computer-aided drawing model

the damage from accumulated fatigue using the reservoir or rainflow method (Baek et al. 2008). In addition, the reliability calculation of the crane has been performed by counting the number of fatigue defects found after a non-destructive inspection.

In the present study, dominant design variables to be used in the structural size optimization are extracted via an orthogonal-array-based sensitivity analysis. Response surface models are first established using a central composite design (CCD) in the context of design of experiments (DOE). An approximate deterministic optimization (DO) solution is obtained using such response surface method based on a second-order polynomial. Further, to accommodate uncertainties in the design, such as material properties,

dimensional tolerance, and external loading conditions, reliability based design optimization (RBDO) is conducted to assess the probability of failure in terms of stress and defection constraints. Optimal design solutions calculated from DO and RBDO are compared, including an evaluation of the DO and RBDO solutions under severe loading conditions.

2 LLC mechanism analysis

Herein the trajectory motion is considered of the four-bar planar structure that describes the operation of the LLC. All the geometric magnitudes of a four-bar mechanism are shown in Fig. 2. A positional analysis of the four-bar mechanism can be performed using the closed equations shown below.

$$r_2 \sin\theta_2 + r_3 \sin\theta_3 = r_4 \sin\theta_4 \tag{1}$$

$$r_2 \cos\theta_2 + r_3 \cos\theta_3 = r_1 + r_4 \cos\theta_4 \tag{2}$$

The unknowns in (1) and (2) are θ_3 and θ_4, which can be calculated from an input angle θ_2 and Freudenstein's equation. Then, the coupler coordinates (C_{Xr}, C_{Yr}) can be expressed as in (3) and (4) on the basis of the reference coordinate of Fig. 2:

$$C_{Xr} = r_2 \cos\theta_2 + r_x \cos\theta_3 - r_y \sin\theta_3 \tag{3}$$

$$C_{Yr} = r_2 \sin\theta_2 + r_x \sin\theta_3 + r_y \cos\theta_3 \tag{4}$$

As just mentioned, the value of $\theta_3$can be calculated from an input angle $\theta_2$and Freudenstein's equation:

$$\theta_3 = 2\tan^{-1}\left(\frac{-E \pm \sqrt{E^2 - 4DF}}{2D}\right) \tag{5}$$

$$D = \cos\theta_2 - k_1 + k_4 \cos\theta_2 + k_5 \tag{6}$$

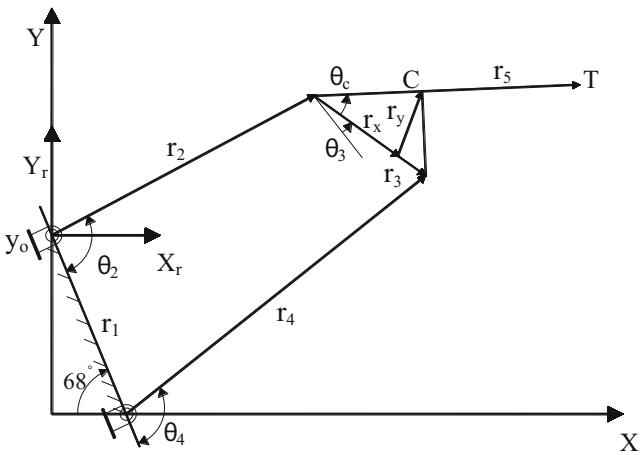

Fig. 2 Four-bar mechanism of double-rocker

$$E = -2\sin\theta_2 \tag{7}$$

$$F = k_1 + (k_4 - 1)\cos\theta_2 + k_5, \tag{8}$$

where $k_1 = \frac{r_1}{r_2}$, $k_4 = \frac{r_1}{r_3}$, and $k_5 = \frac{r_4^2 - r_1^2 - r_2^2 - r_3^2}{2r_2r_3}$.

Next, the position of the target point based on the reference coordinate system is given as follows; θ_C can be obtained by using the law of cosines:

$$T_{Xr} = C_{Xr} + r_5 \cos(\theta_3 + \theta_C) \tag{9}$$

$$T_{Yr} = C_{Yr} + r_5 \sin(\theta_3 + \theta_C) \tag{10}$$

$$\theta_C = \cos^{-1}\frac{r_x^2 + r_5^2 - r_y^2}{2 \times r_x \times r_5} \tag{11}$$

Thus, the position of target point T, if the translational motion and the rotational motion are added on the basis of the world coordinate system, is defined as:

$$\begin{vmatrix} T_x \\ T_y \end{vmatrix} = \begin{vmatrix} \cos(360-68) & -\sin(360-68) \\ \sin(360-68) & \cos(360-68) \end{vmatrix} \begin{vmatrix} T_{xr} \\ T_{yr} \end{vmatrix} + \begin{vmatrix} 0 \\ 13,200 \end{vmatrix} \tag{12}$$

Now, the trajectory as a function of the path generation of the target point in (12) is to be prescribed. The planar mechanism of the double-rocker has a two-dimensional motion undergoing both translation and rotation as shown in Fig. 2. The double-rocker rotates 68 deg clock-wise to create 292 (= 360-68) deg; the position of y_o is translated 13,200 mm in the y-direction and does not move in the x-direction, which is described as a vector of $[0, 13{,}200]^{\mathrm{T}}$ in (12). In the present study, a total of seven links, denoted r_1~r_5, r_x, and r_y are used to prescribe the trajectory mechanism with θ_2 as an input angle. The initial baseline values used herein are r_1 = 14,200 mm, r_2 = 23,000 mm, r_3 = 6300 mm, r_4 = 27,400 mm, r_5 = 13,200 mm, r_x = 5900, r_y = 1500 m, based on the real LLC structure and input angles ranging from 92 to 128°. The trajectory path using these values is shown in Fig. 3, and the results of the path generation are listed in Table 1.

3 LLC trajectory design

3.1 Design sensitivity

The purpose of the LLC trajectory optimization is to minimize the range in the vertical amplitude of a linkage. Seven links ($r_1 \sim r_5, r_x r_y$) are necessary to generate the trajectory. These links become the design variables, and out of these, r_1 is established as the ground. Therefore, there are effectively six variables ($r_2 \sim r_5, r_x r_y$) to be used in

designing the trajectory. The present study further conducts the DOE based sensitivity analysis to extract more dominant design variable from initial six design candidates. The design level is established in Table 2, and orthogonal array data results are given in Table 3. The factor effects of analysis of means (ANOM) based sensitivity analysis (Lee and Kwon 2013) are shown in Fig. 4, wherein two parameters of r_5 and r_x has relatively less influence on the moving distance and the amplitude of trajectory; thus, these variables were excluded from further consideration, and the optimization was carried out using the remaining four variables, $r_2 \sim r_4$ and r_y.

4 Formulation of trajectory optimization

The objectives of this study are to reduce the amplitude of the trajectory and to optimize the length of the links of the four-bar linkage As the 'amplitude in the y-direction' (i.e., the vertical distance) of a LLC mechanism gets increased, the repeated loading to a structure becomes more cumulative and the operating time is increased as well. In this consequence, the vertical amplitude of the trajectory is to be minimized in the present study. The objective function and design constraints for length optimization are as follows:

$$\text{Minimize} \quad \text{Amplitude in y-direction} \tag{13}$$

$$\text{Subject to } 35,798 \text{ mm} \leq x\text{-direction} \leq 40,398 \text{ mm for loading to vessel} \tag{14-1}$$

$$13,759\text{mm} \leq \text{x-direction} \leq 15,759\text{mm for unloading from port} \tag{14-2}$$

$$22,500 \leq r_2 \leq 23,500,\ 6,100 \leq r_3 \leq 6,500 \text{(unit: mm)}$$
$$26,800 \leq r_4 \leq 27,800,\ 1,300 \leq r_y \leq 1,700$$

The LLC structure is moving based on the double-rocker mechanism and its trajectory is generated according to an input angle. The objective function in the trajectory optimization is the vertical amplitude during the loading/unloading trajectory between vessel and port. Constraint conditions of (14-1) and (14-2) are allowable positions for the loading to vessel and the unloading from port as shown in Fig. 1 (b). As mentioned before, the initial design has $r_2 = 23{,}000$ mm, $r_3 = 6300$ mm, $r_4 = 27400$ mm, and $r_y = 1500$ mm. The trajectory including three important points is shown in Fig. 5; in addition to the moving distance (x-distance) of the trajectory, the constraints on the movement points A and C are presented in the figure. In the Cartesian coordinate system, the trajectory curve is created according to an input angle of the double-rocker mechanism. The moving distance is the horizontal range between points A and C in the x-direction, and the amplitude is the vertical distance between points A and B in the y-direction as shown in Fig. 5. Here, the three points A, B and C correspond to the loading point, the highest point between loading and unloading, and the unloading point, respectively. The point A corresponds to the loading/unloading position at the vessel. Since the vessel can be movable due to the wave, it is possible for the point A to move to the right and upward. Movement to the left and right from the bottom is possible because this is the position to load and unload to the ground at point C. The tolerance range has been selected to be from 2,300 to +2,300 mm for loading to the vessel and -1,000 to +1,000 mm for unloading from the port. Also, movements to left right and down are possible from point B.

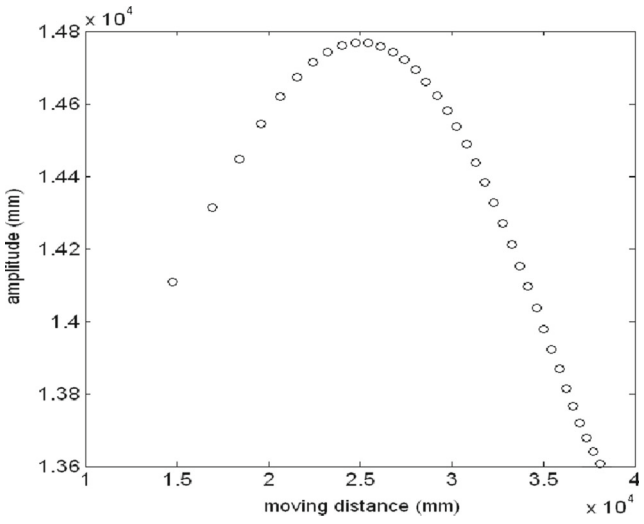

Fig. 3 Target point trajectory: an initial design

The trajectory optimization is conducted via full factorial design (FFD) based kinematic analysis such that design variable values are selected as $r_2 = (22500, 23000, 23500)$, $r_3 = (6100, 6300, 6500)$, $r_4 = (26800, 27400, 27800)$, $r_y = (1300, 1500, 1700)$ as shown in Table 2. That is, this is a FFD with four-factor and three-level resulting in a total of $3^4 = 81$ evaluations. An optimal solution is finally identified as the objective function value is minimized under constraint conditions satisfied.

Table 1 Result of target point trajectory

Classification	Min. (mm)	Max. (mm)	Max – Min (mm)
Moving distance (x)	14,758.8	38,098.2	23,339.4
Amplitude (y)	13,607.2	14,768.1	1,160.9

Table 2 Trajectory design parameters: factors and levels

Level	r_2	r_3	r_4	r_6	r_x	r_y
0	22,500	6,100	26,800	12,700	5,700	1,300
1	23,000	6,300	27,400	13,200	5,900	1,500
2	23,500	6,500	27,800	13,800	6,100	1,700

Table 3 Orthogonal array data for trajectory design

Run	r_2	r_3	r_4	r_6	r_x	r_y	Moving distance (X-dir. mm)			Amplitude (Y-dir. mm)			Gradient (dy/dx)	
							Max	Min	Max-Min	Max	Min	Max-Min	Max	Min
1	0	0	0	0	0	0	36,609	15,791	20,818	14,146	13,065	1,081	0.057	–0.124
2	0	0	1	1	1	1	38,316	14,622	23,694	15,259	14,211	1,048	0.126	–0.067
3	0	0	2	2	2	2	39,723	15,379	24,344	16,197	14,334	1,862	0.209	–0.017
4	0	1	0	0	2	2	37,441	15,218	22,224	14,555	13,572	983	0.108	–0.127
5	0	1	1	1	0	0	37,860	12,113	25,747	15,494	14,395	1,099	0.112	–0.126
6	0	1	2	2	1	1	39,295	13,809	25,486	16,168	14,667	1,501	0.174	–0.075
7	0	2	0	0	1	1	36,998	15,675	21,323	14,883	13,263	1,620	0.094	–0.189
8	0	2	1	1	2	2	38,628	15,098	23,530	16,012	14,876	1,136	0.167	–0.132
9	0	2	2	2	0	0	38,846	12,196	26,649	16,359	14,999	1,360	0.164	–0.133
10	1	1	0	1	1	2	37,537	17,585	19,952	13,592	12,508	1,084	0.077	–0.141
11	1	1	1	2	2	0	38,386	14,113	24,273	13,730	12,575	1,156	0.066	–0.125
12	1	1	2	0	0	1	38,065	14,569	23,496	16,412	15,144	1,268	0.128	–0.148
13	1	2	0	1	0	1	37,087	15,465	21,622	13,964	12,251	1,713	0.065	–0.205
14	1	2	1	2	1	2	38,929	16,534	22,396	14,944	13,805	1,139	0.133	–0.141
15	1	2	2	0	2	0	37,958	11,948	26,010	15,997	14,103	1,894	0.100	–0.193
16	1	0	0	1	2	0	36,870	15,631	21,239	12,541	11,316	1,225	0.013	–0.129
17	1	0	1	2	0	1	38,565	16,597	21,967	14,179	13,511	668	0.096	–0.076
18	1	0	2	0	1	2	38,499	16,357	22,142	16,149	15,210	939	0.138	–0.086
19	2	2	0	2	2	1	37,336	14,886	22,451	12,247	10,451	1,796	0.018	–0.204
20	2	2	1	0	0	2	37,664	15,849	21,815	15,314	13,515	1,799	0.094	–0.224
21	2	2	2	1	1	0	38,071	13,998	24,073	15,072	13,033	2,039	0.066	–0.209
22	2	0	0	2	1	0	36,802	16,104	20,697	11,665	10,166	1,499	-0.015	–0.142
23	2	0	1	0	2	1	37,501	16,022	21,479	13,841	12,597	1,244	0.037	–0.140
24	2	0	2	1	0	2	38,706	16,019	22,687	15,152	14,316	836	0.108	–0.098
25	2	1	0	2	0	2	37,625	18,115	19,510	12,547	11,403	1,143	0.050	–0.152
26	2	1	1	0	1	0	37,038	16,196	20,843	14,265	12,327	1,938	0.024	–0.201
27	2	1	2	1	2	1	38,543	16,102	22,441	14,710	13,377	1,333	0.078	–0.148

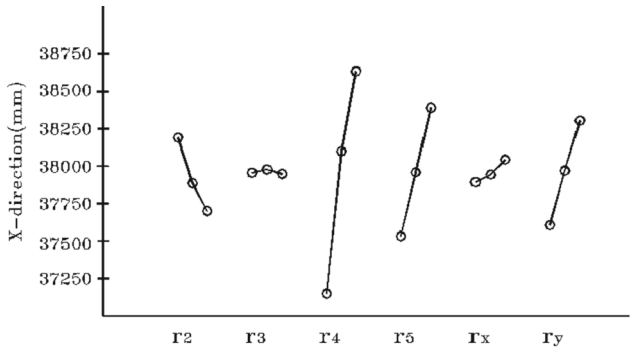

(a) Max in x-direction

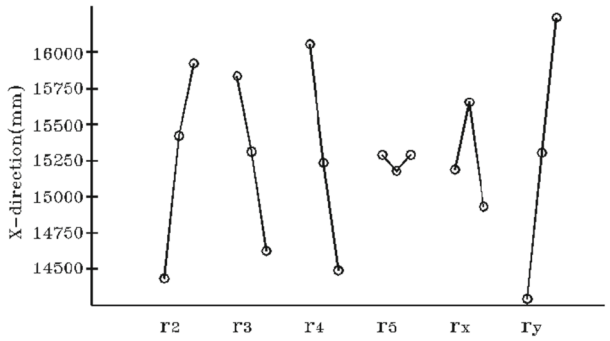

(b) Min in x-direction

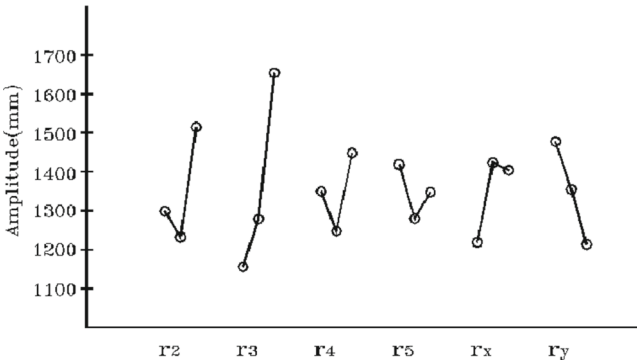

(c) Amplitude

Fig. 4 Sensitivity analysis for trajectory optimization

4.1 Results of trajectory Optimization

When optimizing the length of the link to reduce the amplitude of the trajectory while satisfying the constraints on the range of the moving distance, the objective function value should become smaller than the standard length for trajectory generation because the stress and the deflection increases later when the structural analysis is implemented on the basis of this length Therefore, if the length of r_2 were decreased while holding the remaining three variables at their baseline values, the trajectory would move upward. Conversely, decreasing the lengths r_3, r_4, and r_y as much

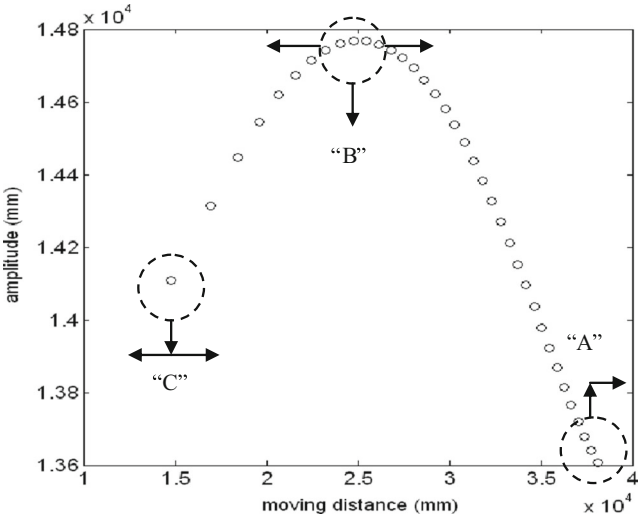

Fig. 5 Target point trajectory and moving constraints of points A, B, C

as possible moves the whole trajectory to the bottom. Here, r_y has been excluded as a design variable because its basic length is small; also, the choice between r_2 and r_4 is arbitrary because reducing both these lengths simultaneously has no effect on the trajectory. Accordingly, r_2 and r_3 have been selected as the final design variables. Reducing the length of r_2 and r_3 to optimize the length of the symmetric parabola while staying within the constraints imposed on points A and C yields the values $r_2 = 22{,}875$ mm and $r_3 = 6165$ mm. The graph is shown in Fig. 6 and the resulting values are listed in Table 4. As a result of the optimization, the values are in the error range (min: 3.18 %, max: 0.2 %) of the target point viewed from the side of the mov-

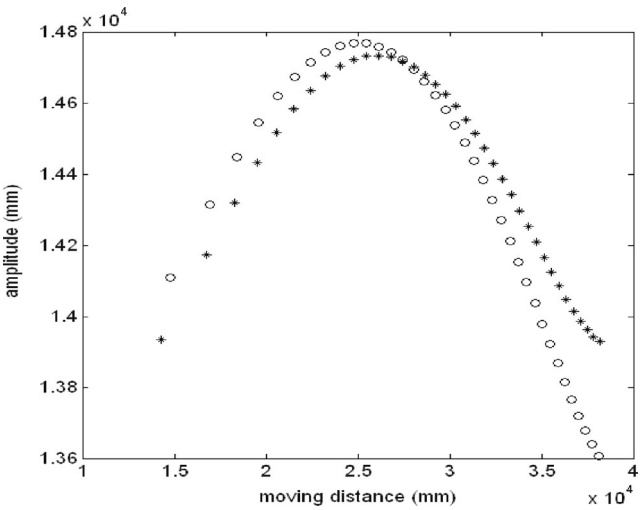

Fig. 6 Results of curve. (o): initial; (*): optimal

Table 4 Comparison of initial, optimal and measured results

	r_2	r_3	r_4	r_y	Moving distance (mm)			Amplitude (mm)			Rotation angle (deg)
					Min	Max	Max-Min	Min	Max	Max-Min	
Initial	23,000	6,300	27,400	1,500	14,758.8	38,098.2	23,339.4	13,607.2	14,768.1	1,160.9	92 ∼ 128
Optimal	22,875	6,165	27,400	1,500	14,289.3	38,174.0	23,884.7	13,928.9	14,733.1	804.2	92 ∼ 128
Measured	22,875	6,165	27,400	1,500	14,246.1	38,131.6	23,885.5	13,754.7	14,533.9	779.2	92 ∼ 128

ing distance compared with the existing fourbar mechanism structure. The final amplitude (804 mm) decreases by nearly 31 % from the baseline amplitude (1161 mm) according to the kinematic movement. This optimization result could be advantageous when it is applied to the actual structure. The shipment location of a vessel may either decrease or increase due to external factors (waves, the position of the vessel's berth, etc.) when the portage is loaded and unloaded using the real structure (i.e., the LLC). This locational tolerance can be satisfied if the moving distance increases In addition, if the amplitude decreases as the length of each link decreases, then the length of optimized link becomes significant in this situation since the deflection and stress decrease for the same load. Strengthbased size optimization based on the result of this trajectory optimization will be discussed after the numerical optimization result in the trajectory design is compared with actual LLC measurement in the next section.

Methods by E. J. Haug, et al. [10-12] have conducted position, velocity and acceleration analysis using the kinematic equations (i.e., cost function). Once the constraint function is provided, the optimal solution can be obtained through a traditional nonlinear programming. Also, the variation of state variables is available via the sensitivity analysis. While such mathematical process has an advantage of the integrated kinematic analysis, design and optimization, it requires the difficulty in formulating and solving differential-algebraic equations. Instead the present study identifies an optimized trajectory design simply using orthogonal array data, ANOM based sensitivity analysis and additional 81 function evaluations of full factorial design, without depending on complex differential-algebraic equations.

4.2 Verification with real model measurement

In this section, the trajectory design solution obtained from the numerical mechanism analysis and optimization process is compared to the trajectory of the LLC to which the actual length of link has been applied The actual model is the LLC equipment installed and used at the Mokpo port in Korea, and the length of the optimized link is applied and installed in the fly jib, back stay, and main jib sections In the trajectory test, a three-dimensional light wave instrument GPT-7502 2011 is used to measure the LLC trajectory under unloading operating conditions. The value of the coordinate transformation is measured based on the angular change by establishing the center of the lower hinge pin of the main jib as the starting point and establishing the target at the center of hinge pin of the end point of the end jib as shown in Fig. 7 The test model for the measurement is the same as the actual LLC depicted in Fig. 1 **a**. The measurement interval of the end point is a 5 deg input angle. The numerical trajectory optimization result is compared with

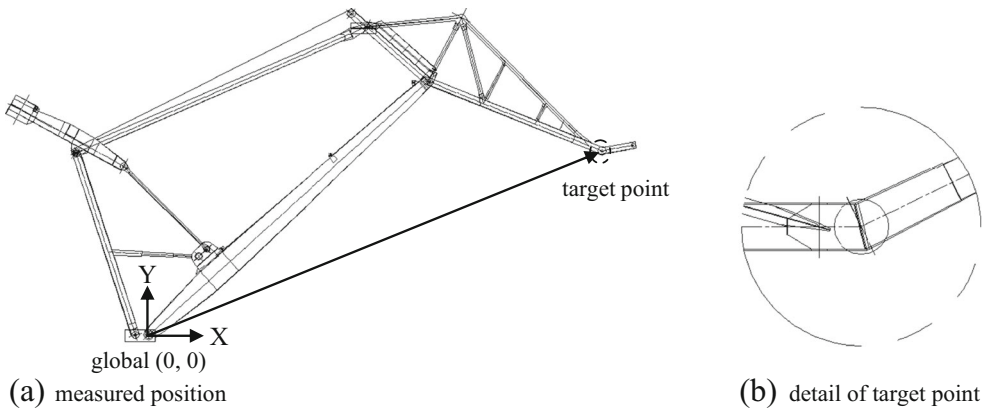

Fig. 7 Three-dimensional coordinate positions for measurement

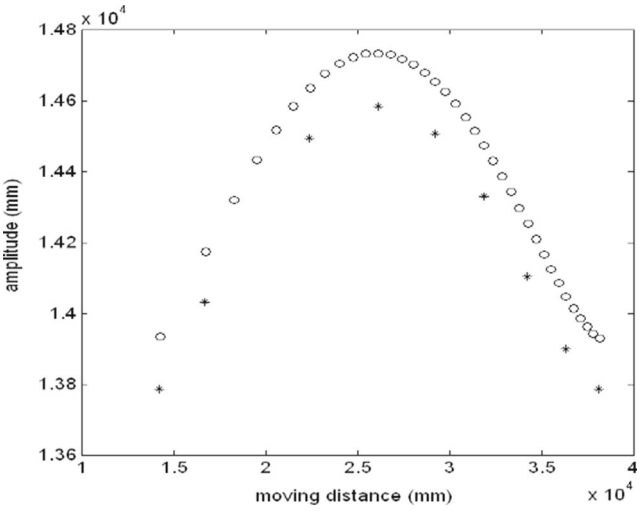

Fig. 8 Results of curve. (o): optimal; (*): measured

measured data by using the target point value obtained from the three-dimensional light wave instrument. The graph of the numerical optimization result and its test measurement is shown in Fig. 8, and the data are listed in Table 4. The difference between the optimized and actual measured values of the length is only 42.4 mm (= 38174.0 mm – 38131.6 mm) for the maximum moving distance and 199.2 mm for the amplitude Such deviation appears high due to the deflection by the dead load; as identified in finite element analysis, the pure deflection by the dead load is 176.4 mm. Despite this difference between the measured value and the numerical optimization result, it may be understood that the configuration of two trajectory results is similar.

4.3 Design process

To implement actual loading conditions, finiteelementbased structural modeling and analysis is conducted to evaluate stress and deflection of the LLC structure both when it is in service and out of service. Then, the DO is formulated such that the weight of the LLC structure is minimized subjected to inequality constraints on structural strength such as von Mises stress and deflection. Prior to this size optimization, a design sensitivity analysis is employed to extract the dominant design variables from candidate design variables. In the numerical optimization process, to carry out approximate optimization, a response surface method based on a second-order polynomial is used. Further, because of the design uncertainties present in an actual environment, reliability based design optimization (RBDO) is explored to assess the probability of failure in terms of stress and deflection. Finally, the solutions obtained by using DO and RBDO are evaluated under severe loading conditions to examine their design safety.

4.4 Loading conditions

The load acting on the LLC may be classified into two main types First, there is a lifting load and a horizontal load on the LLC when it loads and unloads the portage (the sand, the iron mineral, etc.), moving it between the vessel and the ground. Second, there are external forces such as wind load and seismic load that do not originate from the basic loading and unloading processes International standards concerning the application of wind load and earthquake load are applied herein Here, the codes JIS B 8821 2004 and BS 2573 1983 are observed, and various loads are determined as shown in (15) through (19):

$$Self - weight = 1.0 \times (acceleration\ of\ gravity) \quad (15)$$

$$Lifting\ load = 10ton \quad (16)$$

$$Level\ luffing\ load = \beta \times (lifting\ load) \quad (17)$$

$$Wind\ load = F_w = \gamma \times A \times q \times C_f \times \phi^{(n-1)} \quad (18)$$

Table 5 Comparison of initial, optimal and measured results

Load	In service		Out of service			
	Case 1	Case 2	Case 3	Case 4	Case 5	Case 6
Self-weight	1	1	1	1	1	1
Lifting	1	1	–	–	–	–
Level luffing motion	1	1	–	–	–	–
Wind (v=25m/s, x-dir.)	1	–	–	–	–	–
Wind (v=25m/s, z-dir.)	–	1	–	–	–	–
Wind (v=60m/s, x-dir.)	–	–	1	–	–	–
Wind (v=60m/s, z-dir.)	–	–	–	1	–	–
Seismic (x-dir.)	–	–	–	–	1	–
Seismic (z-dir.)	–	–	–	–	–	1

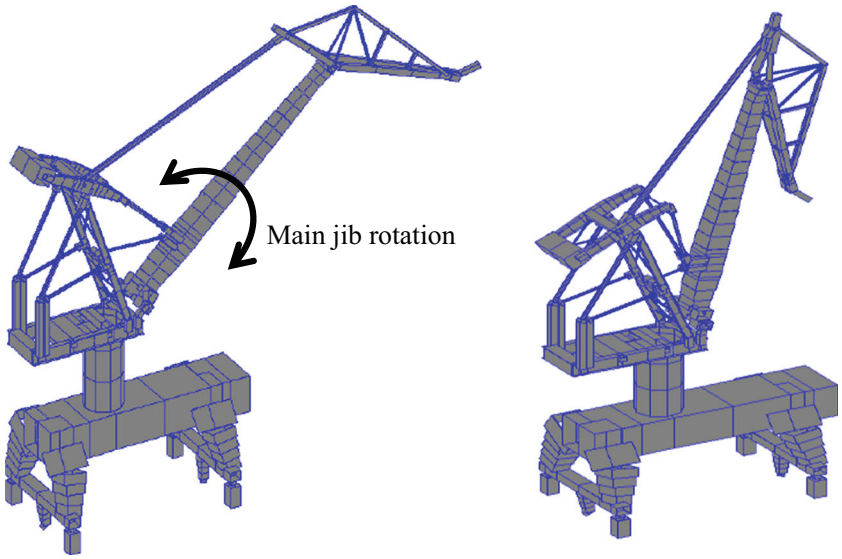

(a) In service (b) Out of service

Fig. 9 structural models for in-service and out of-service

where $\beta = 0.01\sqrt{V}$ (where, V = 20 meter/minute), F_w is the wind load, γ is a factor related to the design application of the calculated wind load (for structural calculation, $\gamma = 1.0$), A is the effective frontal area, $q$is the wind pressure corresponding to the appropriate design condition, $C_f$is the force coefficient in the direction of the wind, and ϕ is a shielding factor that is determined by the solidity ratio of the front frame and the spacing ratio. Also, the load combination conditions for each individual load are listed in Table 5.

$$Seismic\ load = 0.2 \times (self\ weight) \tag{19}$$

Based on the provisions of the Korean Harbor Act and the international codes (JIS and BS), the load combination conditions listed in Table 5 are classified as either in service or out of service. The wind load is separated in the X and Z directions because the area acting on the wind power varies according to direction, thereby causing the wind load to vary with direction The seismic momentum force is also accounted for in terms of the X and Z directions because the applied load differs with direction. The value of 1 in Table 5 is the scaling factor The worst case load is varied according the coordinate system. The present study conducts the structural analysis and design based on KS (Korea Standard), JIS (Japan Industrial Standard) and BS (British Standard).

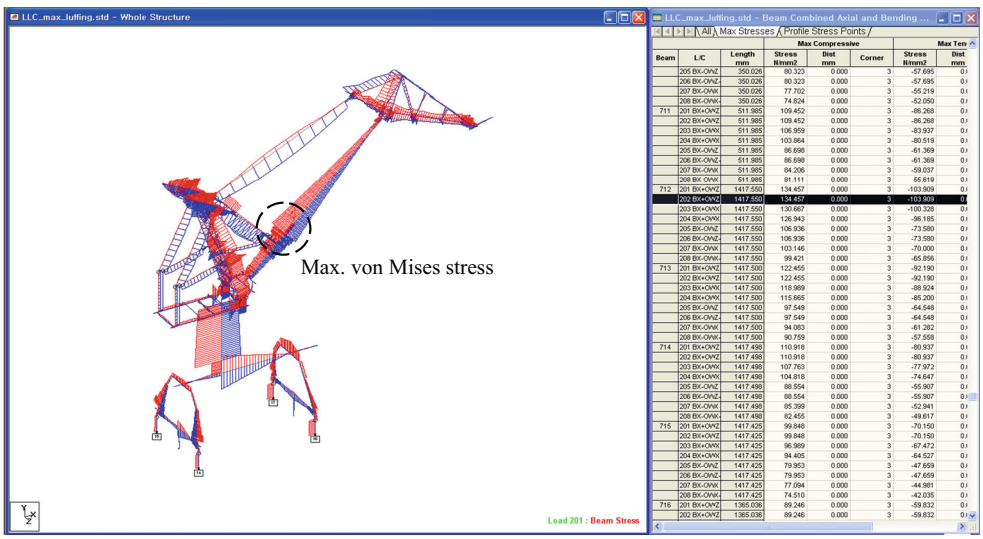

Fig. 10 Analysis result of von Mises stress for in-service

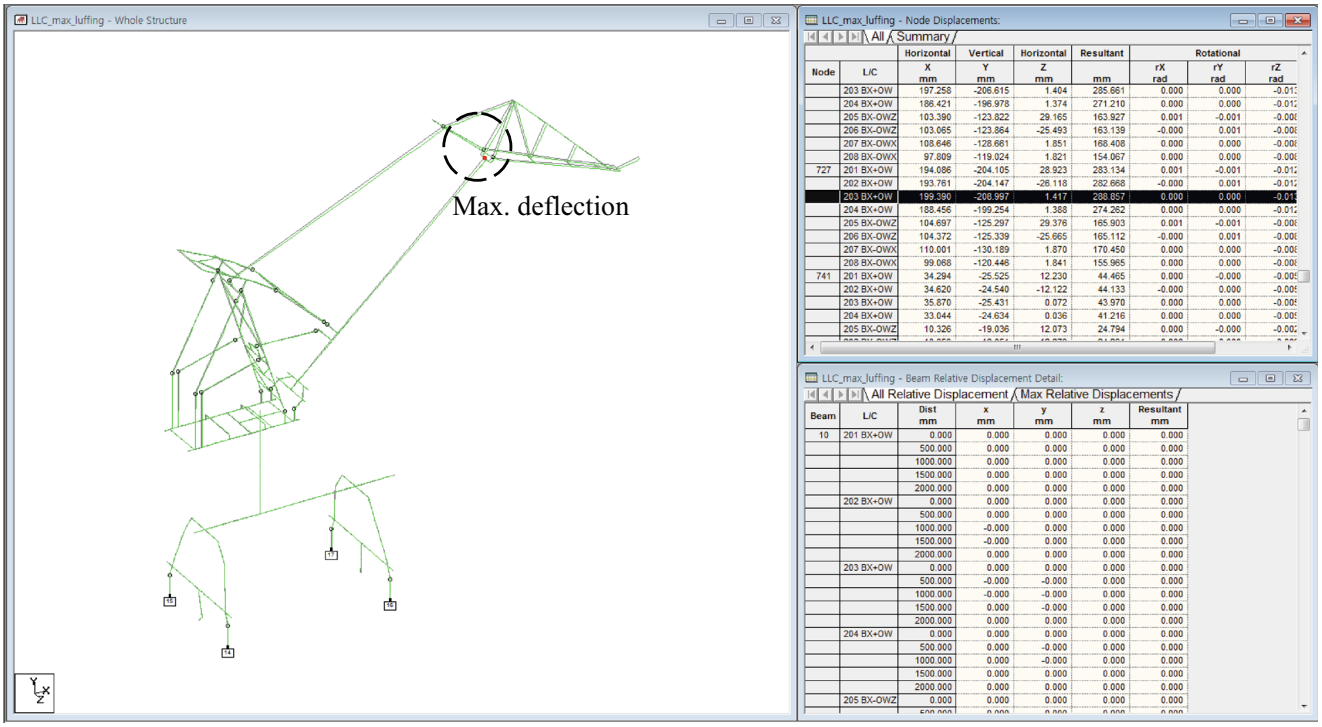

Fig. 11 Analysis result of deflection for in-service

Such standards recommend applying the same value(s) of the worst caseload.

5 Strengthbased LLC design

5.1 Structural modeling and analysis

The finite element method (FEM) program used for the structural analysis is STAAD.PRO (STAAD.PRO 2004), which has been developed for the structural analysis of harbor equipment such as steel structures and cranes. This program is widely used in many countries for structural analysis. The beam configuration modeling applied to implement the structural analysis and the configurations for in-service and out-of-service conditions are shown in Fig. 9. Implementing the structural analysis, including the classification of in service or out of service according to the load combination conditions, results in the maximum stress shown in Fig. 10, and the maximum deflection shown in Fig. 11; the data resulting from final analysis are listed in Table 6. The moving mechanism of a LLC structure consists of main jib, back stay and fly jib as shown in Fig. 1(b). The main jib supports the LLC structure. The back stay that is connected with the fly jib allows the fly jib to move via motor rotation. The fly jib unloads the portage at the specified position such as vessel and/or port (ground). In the structural analysis result for each of load cases, stress and deflection are found to be maximized when the luffing angle is at its maximum; Case 2 has the maximum stress and Case 1 has the maximum deflection. Accordingly, the optimization is implemented under these two cases (i.e.,

Table 6 Summary of FEA result for each load case

Load case	Location	Stress (N/mm^2)	Location	Deflection (mm)
Case 1	Main jib	130.667	Main jib	208
Case 2	Main jib	134.457	Main jib	204
Case 3	Main jib	96.915	Back stay	36
Case 4	Fly jib	114.116	Back stay	7
Case 5	Fly jib	32.711	Main jib	29
Case 6	Fly jib	59.868	Back stay	7

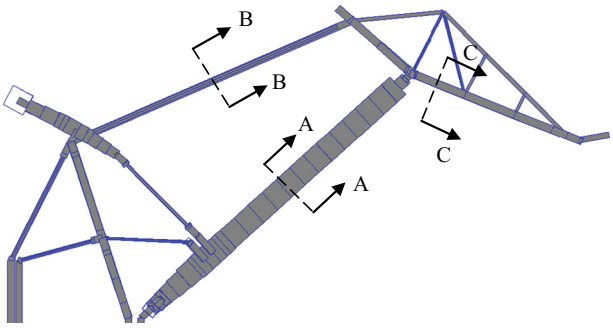

Fig. 12 Positions of three cross-sections

Case 1 and Case 2) to accommodate the risks in this design environment.

5.2 Formulation of strength-based optimization

The design variables are established for the cross section for the double-rocker structure; the designated position of the cross section and a detailed drawing are shown in Figs. 12 and 13 respectively Therefore, the total number of design variables for each becomes eight If the weight of the structural section of the double-rocker configuration increases in all LLC models, the weight of the counterweight will also increase.

Therefore, the stress and deflection are established as the constraints by designating the minimization of weight as an objective function

$$\text{Minimize} \quad W(x_i) \quad i = 1, 2, 3, \ldots\ldots, 8 \tag{20}$$

$$\text{Subject to} \quad g_1(x_i) = von\ Mises\ stress - 180\,N/mm^2 \le 0 \tag{21}$$

$$g_2(x_i) = deflection - \left(\frac{span}{500} = \frac{27,400mm}{500} = 54.8mm\right) \le 0$$

$$1,823 \le x_1 \le 1,863, \quad 1,747 \le x_2 \le 1,787 (unit : mm)$$

$$11.0 \le x_3 \le 13.0, \quad 498.0 \le x_4 \le 518.0$$

$$8.0 \le x_5 \le 10.0, \quad 380.0 \le x_6 \le 400.0$$

$$556.0 \le x_7 \le 576.0, \quad 7.0 \le x_8 \le 9.0 \tag{22}$$

The amount of deflection in (22) is the constraint on the applied external load excluding the dead load of the structure. The dead load (i.e., self-weight) is considered during the structural analysis as shown Table 5. However, the dead load is not included in the deflection constraint in order to accommodate only the elastic behavior of LLC structure. That is, the present study does not consider the plastic behavior due to both applied loading and dead weight. Since the amount of deflection of the main jib is the highest in the doublerocker structure the main jib is employed for the deflection constraint. Here, the applied span of the main jib is 27,000 mm. The values of deflection are classified as the total deflection, the dead load and the external load. The dead load is related to the amount of deflection by the pure dead load, the external load is related to the amount of deflection by the load excluding the dead load and the total deflection is associated with the sum of these two weights.

5.3 Sensitivity analysis

The calculation time increases when the optimization uses all eight design variables, but it can be decreased by selecting more significant design variables based on DOE based ANOM as used in the trajectory optimization. The level and factor for design of experiments (DOE) are shown in

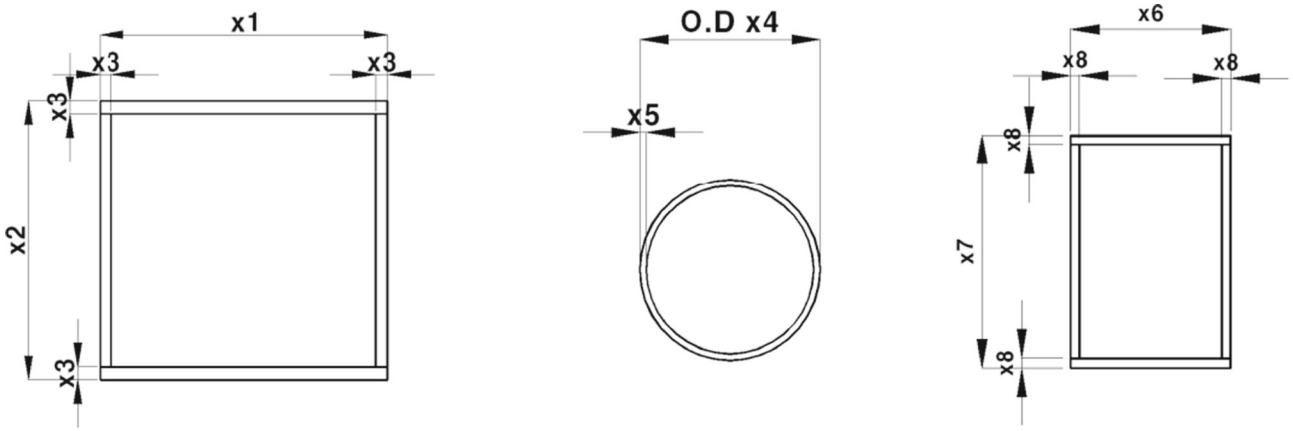

(a) section A-A(main jib) (b) section B-B(back stay) (c) section C-C(fly jib)

Fig. 13 Thickness dimensions of each cross section

Table 7 Structural design variables: factors and levels

Level	x1	x2	x3	x4	x5	x6	x7	x8
	1823	1747	11	498	8	380	556	7
1	1843	1767	12	508	9	390	566	8
2	1863	1787	13	518	10	400	576	9

Table 7, and the corresponding FEM results of von Mises stress and deflection using an orthogonal array are listed in Table 8. The ANOM used to determine sensitivity is based on the table of orthogonal arrays and the result of the structural analysis, as shown in Fig. 14. Thus, x_3 and $x_8$are selected as the final design variables. x_1 and $x_2$are also selected because section A-A(main jib) is the most important section supporting the entire load of the LLC's doublerocker structure. Therefore, from the total of eight candidate design variables, the four variables x_1, x_2, x_3, and x_8 are selected as the actual design variables to be studied

5.4 Deterministic optimization

The response surface meta-models (Myers and Montgomery 2009) have been generated using the CCD (Sacks et al. 1989) to find the approximate optimal solution(s). In this study, the second-order regression model is used as the

Table 8 Orthogonal array data for structural design

Run	x1	x2	x3	x4	x5	x6	x7	x8	Weight	Stress	Total deflection
									Ton	N/mm^2	mm
1	0	0	0	0	0	0	0	0	60.274	131.853	201
2	0	0	1	1	1	1	1	1	63.929	130.448	213
3	0	0	2	2	2	2	2	2	67.644	129.457	225
4	0	1	0	0	1	2	2	2	64.257	143.928	221
5	0	1	1	1	2	0	0	0	62.138	124.02	203
6	0	1	2	2	0	1	1	1	65.803	121.072	212
7	0	2	0	0	2	1	1	1	62.397	136.716	211
8	0	2	1	1	0	2	2	2	66.131	132.627	220
9	0	2	2	2	1	0	0	0	64.023	115.227	203
10	1	0	0	1	0	0	1	2	63.789	142.365	219
11	1	0	1	2	1	1	2	0	62.503	125.056	205
12	1	0	2	0	2	2	0	1	65.803	122.815	215
13	1	1	0	1	1	2	0	1	62.397	136.684	211
14	1	1	1	2	2	0	1	2	65.664	133.529	221
15	1	1	2	0	0	1	2	0	64.387	115.802	205
16	1	2	0	1	2	1	2	0	60.961	131.019	203
17	1	2	1	2	0	2	0	1	64.281	126.063	210
18	1	2	2	0	1	0	1	2	67.557	123.480	220
19	2	0	0	2	0	0	2	1	62.397	136.629	211
20	2	0	1	0	1	1	0	2	65.664	133.086	220
21	2	0	2	1	2	2	1	0	64.387	117.893	208
22	2	1	0	2	1	2	1	0	60.961	130.929	203
23	2	1	1	0	2	0	2	1	64.281	127.888	213
24	2	1	2	1	0	1	0	2	67.557	123.485	220
25	2	2	0	2	2	1	0	2	64.111	140.012	219
26	2	2	1	0	0	2	1	0	62.855	120.479	202
27	2	2	2	1	1	0	2	1	66.184	118.763	213

model of the response surface The objective function and constrained function values obtained by the CCD and corresponding to four design variables are listed in Table 9. Response surface models can be obtained for the weight, the stress and the amount of deflection using (23) through (25) as follows:

$$\begin{aligned} W_{weight} = {} & 1.3720E^{-6} + 1.6025E^{-2}x_1 + 1.6401E^{-2}x_2 \\ & +4.5552E^{-2}x_3 + 1.6998x_8 - 3.7881E^{-6}x_1^2 \\ & -4.0271E^{-6}x_2^2 - 2.4074E^{-3}x_3^2 - 4.7789E^{-3}x_8^2 \\ & -1.1203E^{-6}x_1x_2 + 4.8901E^{-4}x_1x_3 \\ & -9.4107E^{-6}x_1x_8 + 4.8296E^{-4}x_2x_3 \\ & -3.0303E^{-6}x_2x_8 + 1.1677E^{-4}x_3x_8 \end{aligned} \tag{23}$$

$$\begin{aligned} g_{stress} = {} & 3.3760E^{-5} + 2.8586E^{-1}x_1 + 1.3875E^{-1}x_2 \\ & -33.840x_3 + 20.592x_8 - 8.9868E^{-5}x_1^2 \\ & -6.3684E^{-5}x_2^2 + 6.3124E^{-1}x_3^2 \\ & -4.5056E^{-2}x_8^2 - 1.0290E^{-5}x_1x_2 \\ & +3.0552E^{-3}x_1x_3 - 2.0997E^{-3}x_1x_8 \\ & +4.7913E^{-3}x_2x_3 - 3.5027E^{-3}x_2x_8 \\ & -4.0539E^{-1}x_3x_8 \end{aligned} \tag{24}$$

$$\begin{aligned} g_{deflection} = {} & 3.2127E^{-5} + 2.7376E^{-1}x_1 - 1.6373E^{-2}x_2 \\ & -16.005x_3 + 17.889x_8 - 6.8596E^{-5}x_1^2 \\ & -4.3748E^{-6}x_2^2 + 2.3094E^{-1}x_3^2 \\ & -4.3978E^{-2}x_8^2 - 2.5244E^{-5}x_1x_2 \\ & +2.0765E^{-3}x_1x_3 - 3.8651E^{-4}x_1x_8 \\ & +5.2061E^{-3}x_2x_3 - 3.5085E^{-3}x_2x_8 \\ & -1.8144E^{-1}x_3x_8 \end{aligned} \tag{25}$$

Regarding the accuracy of these approximate metamodels, R^2 values are higher than 99.0% for all three metamodels. The optimization with (20) through (22) using 8 design variables is now replaced by an approximate optimization with (23) through (25) using 4 design variables of x_1, x_2, x_3, and x_8. A method of feasible direction (MFD) (Vanderplaats 1084) has been employed as a gradient based optimizer. The final results are listed in Table 10. It can be seen that the response surface based approximate deterministic optimal solution and its corresponding FEM solution quite similar when the resulting values are compared.

5.5 Reliability based design optimization

The objective in this study is to minimize the weight while satisfying the constraints on stress and deflection of the doublerocker structure. However, because there are inherently uncertain parameters (e.g., material properties, dimensional tolerance, and external loads), reliability based design optimization can be used to determine the reliability by regarding these factors as the probability that a design variable is applied. A method of RBDO seeks the value of the optimal design that satisfies either the reliability index approach (RIA) or the performance measure approach (PMA) [20-22] depending on the analysis technique used Here, the PMA method is applied; it is excellent in terms of calculation speed and convergence.

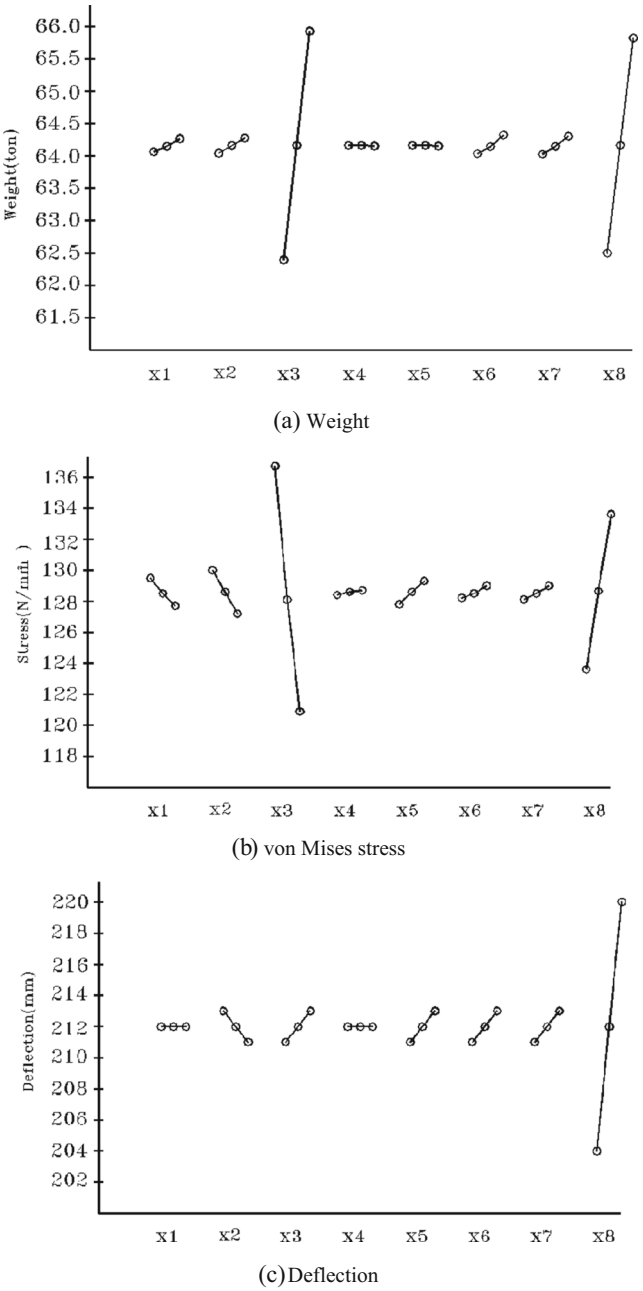

Fig. 14 Sensitivity analysis for structural optimization

Table 9 Central composite design data

Run	x1	x2	x3	x8	Weight	Stress	Deflection (mm)		
					Ton	N/mm^2	Dead load	External load	Total
1	1823	1787	13	9	67.138	127.507	182.2	38.0	220.2
2	1863	1747	13	9	67.138	128.775	186.4	35.5	221.9
3	1863	1787	11	9	63.867	141.866	183.2	34.8	218.0
4	1863	1787	13	7	64.189	116.924	173.4	31.1	204.5
5	1823	1747	13	9	66.884	130.5	186.4	35.5	221.9
6	1823	1787	11	9	63.651	143.803	183.3	34.9	218.2
7	1823	1787	13	7	63.933	118.452	173.4	31.1	204.5
8	1863	1747	11	9	63.651	145.218	184.7	35.4	220.1
9	1863	1747	13	7	63.934	119.616	174.4	31.5	205.9
10	1863	1787	11	7	60.663	131.371	170.9	30.7	201.6
11	1823	1747	11	9	63.436	147.214	184.8	35.5	220.3
12	1823	1747	13	7	63.679	121.19	174.4	31.5	205.9
13	1823	1787	11	7	60.447	133.136	170.9	30.8	201.7
14	1863	1747	11	7	60.447	134.43	172.1	31.3	203.4
15	1823	1747	11	7	60.232	136.248	172.2	31.4	203.6
16	1863	1787	13	9	67.393	125.833	185.3	34.9	220.2
17	1883	1767	12	8	64.032	129.002	178.6	33.1	211.7
18	1843	1807	12	8	64.032	127.761	177.5	32.6	210.1
19	1843	1767	14	8	67.279	117.483	181.4	33.5	214.9
20	1843	1767	12	10	66.987	140.52	190.8	37.0	227.8
21	1803	1767	12	8	63.563	132.486	178.7	33.1	211.8
22	1843	1727	12	8	63.562	133.805	179.9	33.7	213.6
23	1843	1767	10	8	60.306	149.272	177.4	33.2	210.6
24	1843	1767	12	6	60.579	120.824	166.4	29.1	195.5
25	1843	1767	12	8	63.797	130.715	178.6	33.1	211.7

The present study employs second-order polynomials as response surface models. It is practically effective to reduce the number of design variables and use RSM based approximate optimization in the industrial application problem. The weakness of this response surface method based approximate RBDO is such that once the original engineering design problem is highly nonlinear, it is likely for the second-order polynomial based RSM to result in the premature convergence on the optimized solution and to miscalculate the most probable point (MPP) during the RBDO process.

The mathematical statement of RBDO problem is now written as follows:

$$\text{Minimize } W(X_i) i = 1, 2, 3, 8 \tag{26}$$

$$\text{Subject to } P[(G_1(X_i) = g_1) \leq 0] \geq \text{Reliability of } 97.7\% \tag{27}$$

$$P[(G_2(X_i) = g_2) \leq 0] \geq \text{Reliability of } 97.7\% \tag{28}$$

$$X_i^L \leq X_i \leq X_i^U$$

Table 10 Deterministic approximate optimization result and its validation with FEM

	x1(mm)	x2(mm)	x3(mm)	x8(mm)	Weight (ton)	Stress (N/mm^2)	Deflection(mm)		
							Total	Dead load (staad.pro)	External load
DO	1863	1787	12.44	7.0	63.203	120.439	203.5	173.8	203.5 – 173.8 = 29.7
FEM					63.102	118.517	201.7	173.8	201.7 – 173.8 = 27.9

Table 11 Probabilistic design variables for RBDO

	Mean (DO solution)	Lower	Upper	Standard deviation	Distribution type
x1	1,863	1,853	1,873	3.33	Normal
x2	1,787	1,777	1,797	3.33	Normal
x3	12.44	11.44	13.44	0.33	Normal
x8	7.00	6.00	8.00	0.33	Normal

Limit state functions of $G_1(X_i)$ and $G_2(X_i)$ in RBDO are the same as constraints of $g_1(x_i)$ and $g_2(x_i)$ in deterministic optimization, respectively. The stress and the amount of deflection are the probabilistically constrained conditions, with minimum reliability of 97.7%; this reliability figure is determined based on the provisions in BS 5400 (5400 1980). Even though the service life varies depending on the type of the harbor equipment used this equipment generally needs to have a useful life of more than 20 years and thus must be highly reliable

The parameters for the RBDO performance analysis are listed in Table 11, wherein a set of design variable, $X = \{x_1, x_2, x_3, x_8\}$ is considered as probabilistic variables whose types are normal distribution described with mean and standard deviation. The crane is mainly designed based on BS (British Standards Institution), FEM (European Federation of Materials Handling) and JIS (Japanese Standards Association) B 8821 codes, etc. Especially, the BS code recommends the level of 3-sigma for the consideration of probability of material's failure. Therefore, the present study employs the standard deviation values of 3.33 and 0.33 according to the guidance of BS code. Functions of g_{stress} and $g_{deflection}$ are limit state functions in the RBDO formulation. These limit state functions are linearly approximated using the first order second moment (FOSM) based Taylor series expansion to calculate the probabilistic optimal solution. Results from the RBDO are listed in Table 12. The RBDO result shows that the dimension of x_1, x_2representing the width and the height of a main jib's cross section respectively is increased in order to complement a reduction in strength due to a material uncertainty, whereas the thickness of $x_3$and x_8 is decreased in order to reduce a total weight. For reference, the amount of deflection by the dead load obtained through FEM is subtracted from the full amount of deflection obtained through RBDO to check whether constraints are violated on the amount of deflection caused by external forces.

5.6 Effect of load variations

Depending on the location where the equipment is installed, some deviations will arise due to the lifting load, the wind load and the seismic momentum force acting on the LLC Because the lifting load applies the greatest stress to the double-rocker structure, external forces that could cause the equipment to break down need to be estimated by applying load variations to the solutions of DO and RBDO The value of the rated lifting load in the LLC is normally 10 ton. However, such load can be increased as loading/unloading weights (coil, raw materials, steel/chrome steel plate, heavy equipments, etc.) are added. The rated lifting load of 10 ton is a load for coil delivery. Its value is increased to 17˜20 ton for steel delivery and 25˜26 ton for heavier equipment delivery. The rated lifting load is originally 10 ton as shown in (16); here the applied overload weights are 19.5 and 25.5 ton, which are 1.95 and 2.55 times the average load respectively In the present study, RBDO considers design variables as probabilistic variables under each of fixed loading values of 10 ton, 19.5 ton and 25.5 ton. That is, structural thickness is a probabilistic variable and the applied loading is constant. The resulting values are listed in Table 13. It is noted that the stress should be less than 180.0 N/mm^2 and the deflection should be less than 54.8 mm as stated in (21) and (22), respectively. The DO solution exceeded all the constraints under two overload conditions, whereas the RBDO solution exceeded only the deflection constraint for the 25 ton condition only.

Table 12 RBDO with reliability of 97.7% its validation with FEM

	(mm)	x2 (mm)	x3 (mm)	x8 (mm)	Weight (ton)	Stress (N/mm^2)	Deflection (mm)		
							Total	Dead Load (staad. pro)	External load
RBDO	1871	1793	12.43	6.98	63.236	119.613	202.0	172.9	202.0 − 172.9 = 29.1
FEM					62.974	117.787	199.5	172.9	199.5 − 172.9 = 26.6

Table 13 Actual FEM calculations of approximate DO and RBDO solutions

Lifting Load (ton)	Method	x1 (mm)	x2 (mm)	x3 (mm)	x8 (mm)	Weight (ton)	Stress (N/mm^2)	Deflection(mm)			Constraint feasibility
								Total	Dead load	External load	
	DO	1,863	1,787	12.44	7.00	63.203	120.439	203.5	173.8	29.7	feasible
10.0	FEM (DO)	1,863	1,787	12.44	7.00	63.102	118.517	201.7	173.8	27.9	feasible
	RBDO	1,871	1,793	12.43	6.98	63.236	119.613	202.0	172.9	29.1	feasible
	FEM (RBDO)	1,871	1,793	12.43	6.98	62.974	117.787	199.5	172.9	26.6	feasible
19.5	FEM(DO)	1,863	1,787	12.44	7.00	63.102	142.456	228.9	173.8	**55.1**	**infeasible**
	FEM (RBDO)	1,871	1,793	12.43	6.98	62.974	141.368	226.6	172.9	53.7	feasible
25.5	FEM(DO)	1,863	1,787	12.44	7.00	63.102	**180.323**	295.5	173.8	**121.7**	**infeasible**
	FEM(RBDO)	1,871	1,793	12.43	6.98	62.974	179.286	292.9	172.9	**120.0**	**infeasible**

Bold face (with underlined values) means infeasibility in the constraint feasibility in Table 13

6 Concluding remarks

In this study, numerical trajectory optimization in the amplitude of a double-rocker mechanism is explored and the solution of the numerical optimization is compared with the actual measured result. First, the length of the link is reduced compared to an existing structure as the result of optimizing the trajectory of the double-rocker In addition, the amplitude is reduced by about 31%, and the straight-line moving distance is extended The meaning of this optimized solution can be interpreted in two ways. First, if the amplitude is reduced at the same time that the length of the link is reduced, it can be expected that the stress and the amount of deflection will both be reduced relative to when the same external force is applied to the actual structure Second, regarding the increase in straight-line moving distance if the portage is loaded and unloaded from the vessel to the ground by the LLC, the position of loading and unloading may be moved by external factors (e.g., the height of waves or changes in the position of the berth) Therefore, increasing the moving distance is advantageous in allowing the structure to be able to cope with this variable.

When this LLC is manufactured based on the optimized link length, uncertain parameters such as material properties, dimensional tolerance and external loads should also be considered in an actual structure. In a method of RBDO, such uncertain parameters are accommodated through probabilistic design variables in terms of mean and standard deviation and the probability of failure of constraints in terms of performance measure of target reliability. In a comparison of this RBDO solution to that of the DO approach, the use of the DO solution results in damage under overloaded conditions, but the corresponding RBDO solution leads to relatively less undamaged and more stable solutions. Therefore, the present study would suggest that it is necessary to consider the uncertain factors during the structural analysis and design optimization of the level-luffing crane for the design safety and reliability.

Acknowledgments This research is supported by the Basic Science Research Program through the National Research Foundation of Korea (NRF) funded by the Ministry of Education, Science and Technology (2011-0024829).

References

Cabrera JA, Simon A, Prado M (2002) Optimal synthesis of mechanisms with genetic algorithms. Mech Mach Theory 37:1165–1177

Acharyya SK, Mandal M (2009) Performance of EAs for four-bar linkage synthesis. Mech Mach Theory 44:1784–1794

Level Luffing Crane in Mokpo Coal Quay, Jeonnam, Korea (2013)

Moon DH, Hur CW, Choi MS (2009) A study on the link composition design of double link type level luffing jib crane (I). J Korea Soc Power Syst Eng 13(1):19–25

Hur CW, Choi MS, Moon DH (2011) A study on the link composition design of double link type level luffing jib crane (II). J Korea Soc Power Syst Eng 15(1):57–63

Xie LY, James MN, Zhao YX, Qian WX (2010) Reliability analysis for crane boom based on probabilistic finite element method. Adv Mater Res 118(1):502–506

Kim MS, Lee JC, Jeong SY, Ahn SH, Son JW, Cho KJ, Song CK, Park SR, Bae TH (2008) Structure evaluation for the level luffing crane boom. J Korean Soc Mech Eng 32(6):526–532

Baek SH, Cho SS, Joo WS (2008) Fatigue life prediction based on the rainflow cycle counting method for the end beam of a freight car bogie. Int J Automot Technol 9(1):95–101

Lee J, Kwon YS (2013) Conservative multi-objective optimization considering design robustness and tolerance: a quality engineering design approach. Struct Multidiscip Optim 47(2):259–272

Haug EJ, Wehage R, Baman NC (1981) Design sensitivity analysis of planar mechanism and machine dynamics. J Mech Des,ASME Trans 103:560–570

Haug EJ, Wehage R, Baman NC (1982) Dynamic analysis and design of constrained mechanical system. J Mechl Des,ASME Trans 104:778–784

Haug EJ (1984) Analysis, Computer Aided and Optimization of Mechanical System Dynamics. Springer-Verlag, New York, pp 499–554

GPT-7502 (2011) User's manual, TOPCON Company, Tokyo, Japan

JIS B 8821 (2004) Calculation Standards for Steel Structures of Cranes, Japanese Standards Association pp 2–14, Tokyo, Japan

BS 1983 (1983) Part 10: Rules for the Design of Cranes, Specification for Classification, Stress Calculations and Design Criteria for Structures, British Standards Institution, pp. 3-12, London, United Kingdom

STAAD.PRO (2004) Getting started and tutorials research engineers,international division of netGuru, inc., Exton, PA

Myers RH, Montgomery DC (2009) Response surface methodology: process and product optimization using designed experiments. Wiley

Sacks J, Schiller SB, Welch WJ (1989) Designs for computer experiments,Statistical Science,Vol

Vanderplaats GN (1084) Numerical Optimization Techniques for Engineering Design, McGraw-Hill, New York, NY

Song CY, Lee J, Choung JM (2011) Reliability based design optimization of FPSO riser support using moving least squares response surface meta-models. Ocean Eng 38(2-3):304–318

Song CY, Lee J (2011) Reliability based design optimization of knuckle component using conservative method of moving least squares meta-models. Probabilistic Eng Mech 26(2):364–379

Lee J, Song CY (2011) Role of Conservative Moving Least Squares Methods in Reliability Based Design Optimization: A Mathematical Foundation. ASME Tran, J Mech Des 133(12):121005 12

5400 BS (1980) Part 10: Steel, Concrete and Composite Bridges, Code of Practice for Fatigue, British Standards Institution,pp.28-34, London, United Kingdom